PLOS ONE

Petrocarbon evolution: Ramped pyrolysis/oxidation a isotopic studies of contaminated oil sediments from t Deepwater Horizon oil spill in the Gulf of Mexico

Kelsey L. Rogers , Samantha H. Bosman, Mary Lardie-Gaylord, Ann McNichol, Brad E. Rosenheim, Joseph P. M Jeffrey P. Chanton

Published: February 28, 2019 • https://doi.org/10.1371/journal.pone.0212433

Abstract

Hydrocarbons released during the Deepwater Horizon (DWH) oil spill weathered due to exposu During weathering, the hydrocarbons' reactivity and lability was altered, but it remained identifia retention of the distinctive isotope signatures (^{14}C and ^{13}C) of petroleum. Relative to the initial e residue deposited in Gulf sediments based on 2010–2011 data, the overall coverage and quant seafloor has been attenuated. To analyze recovery of oil contaminated deep-sea sediments in t tracked the carbon isotopic composition (^{13}C and ^{14}C, radiocarbon) of bulk sedimentary organi Using ramped pyrolysis/oxidation, we determined the thermochemical stability of sediment orga time series. There were clear differences between crude oil (which decomposed at a lower tem natural hydrocarbon seep sediment (decomposing at a higher temperature; $\Delta^{14}C$ = -912‰) and moderate temperature; $\Delta^{14}C$ = -189‰), in both the stability (ability to withstand ramped temper carbon isotope signatures. We observed recovery toward our control site bulk $\Delta^{14}C$ compositio in ~4 years, whereas sites in closer proximity had longer recovery times. The thermographs als composition of contaminated sediment, with shifts towards higher temperature CO_2 evolution o and loss of higher temperature CO_2 peaks at a more distant site.

Citation: Rogers KL, Bosman SH, Lardie-Gaylord M, McNichol A, Rosenheim BE, Montoya evolution: Ramped pyrolysis/oxidation and isotopic studies of contaminated oil sediments fro in the Gulf of Mexico. PLoS ONE 14(2): e0212433. https://doi.org/10.1371/journal.pone.0212

Editor: Lee W. Cooper, University of Maryland Center for Environmental Science, UNITED S

Received: July 26, 2018; **Accepted:** February 2, 2019; **Published:** February 28, 2019

Data Availability: Data are publicly available through the Gulf of Mexico Research Initiative (GRIIDC) at https://data.gulfresearchinitiative.org, 10.7266/N7KH0KWJ and 10.7266/N7Q52

Funding: This research was made possible by grants from The Gulf of Mexico Research Ini

Ecosystem Impacts of Oil & Gas Inputs to the Gulf (ECOGIG), The Center for the Integrated Gulf Ecosystem (C-Image), and Deep Sea to Coast Connectivity in the Eastern Gulf of Mexi Resuspension, Redistribution and Deposition of DWH Recalcitrant Material (Re-Direct) proje # 521. Funding was also provided by the National Ocean Sciences Accelerator Mass Spectr Graduate Student Internship Program (NSF OCE-1239667). The funders had no role in stud analysis, decision to publish, or preparation of the manuscript.

Competing interests: The authors have declared that no competing interests exist.

Introduction

The results of a number of field studies indicate unambiguously that oil residues from the Deep deposited on the seafloor [1–7]. Of the total oil released, an estimated 0.5–14.4% was deposite Ziervogel [8] argued that these estimates were low because they failed to consider the formatio spread of the surface oil slicks, which could have resulted in a greater extent of seafloor deposi residue was limited to the surface sediment as defined by radiocarbon [3], hopane [1,4], and oth

The severity of impacts on benthic communities depends on the nature of the petroleum-derive the seafloor. It has been suggested that biodegradation and dissolution of oil in the water colum moderated these impacts [5,7,9]. We used ramped pyrolysis oxidation (RPO) to assess the bioc present on the seafloor due to the blowout. With RPO we examined 5 sites in all, 3 contaminate as a function of depth, a control uncontaminated site and a natural seep site. Several studies ha contaminated sediments and have shown a reduction in the overall extent of contamination and Stout et al. [4] and Adhikari et al. [10] showed reduced coverage of elevated levels of hopane a (PAHs) in the years following the blowout. Studies by Stout and Payne [5] and Bagby et al. [9] a multiple hydrocarbons in the sediment, showing that biodegradation continued on the seafloor a sedimented oil-residues. In contrast to focusing on specific petroleum compounds, studies by P Pendergraft and Rosenheim [12] employed ramped pyrolysis/oxidation paired with carbon isoto sediments. We applied their approach to the deep-sea floor.

RPO is an approach to determine the thermochemical stability of organic matter [13]. When pai analysis, the source of the carbon can be inferred as a function of thermal stability. The thermoc based on the amount of energy needed to break the bonds, with higher stability requiring highe bonds break at lower temperatures. The thermal stability of a compound is thus related to its lab substrate in microbially mediated reactions [14]. Fresh crude oil is quite labile, oxidizing at relati degradation leads to oxygenated and higher molecular weight compounds that oxidize at highe DWH event, the oil released into the environment was oxygenated [16], consumed by a variety biomass, burned, or altered in many ways [15,17–19]. We define this altered and unaltered petr petrocarbon [3]. Since portions of this material are no longer amenable to gas chromatographic best method to identify it is isotopically, specifically with radiocarbon [20–22]

Pendergraft et al. [11] linked PAHs, an independent oil tracer, to changes in thermographs (tem products as measured with an infrared gas analyzer) produced from oil contaminated marsh se with elevated PAH content produced different CO_2 thermographs with C isotope signatures indi Pendergraft and Rosenheim [12] studied the evolution of organic carbon over time in oil contam RPO. The thermographs shifted from lower to higher thermochemical stability and correspondir increasing enrichment in both $\delta^{13}C$ and $\Delta^{14}C$ over time, indicating a transformation of the oil as studies show the ability of RPO to detect oil contamination through both the thermographs and CO_2 fractions.

The purpose of this study is to analyze the evolution of the carbon isotopic composition of bulk change in thermochemical composition of sediments at 5 deep-water sites in the northern Gulf the DWH oil spill was indicated by radiocarbon depletion in the bulk organic matter in the surfac With RPO we examined 5 sites: 3 contaminated sites, two in time series and one as a function seep site. We hypothesized that: 1) over time, the bulk isotopic composition of the surface layer to baseline values, 2) the oil-residue deposited in the sediment following the DWH oil spill would fresh Macondo oil and 3) that over time and depth the oil residue would evolve towards greater carbon isotope signatures of the RPO splits were used to infer the origin of the organic material

Materials and methods

Ethics statement: No permissions were required as all sites were in unprotected areas. This fiel or protected species. Oil spill affected sediment was collected in time series from 4 sites (GIP07 2010–2017 and analyzed for bulk radiocarbon. In 2015, we also sampled 4 sites that had conta by Mason et al. [23]. We revisited one of these sites, BP444, again in 2017. Sediment from 5 si (GOM) were analyzed using RPO, including 2 of the time series sites (GIP07 and GIP17), 1 hig (GC600) and 1 non-hydrocarbon influenced control (GB480) site were analyzed using ramped 1). Sediment samples were frozen upon collection, returned to the lab, thawed, treated in 10% freeze-dried and ground.

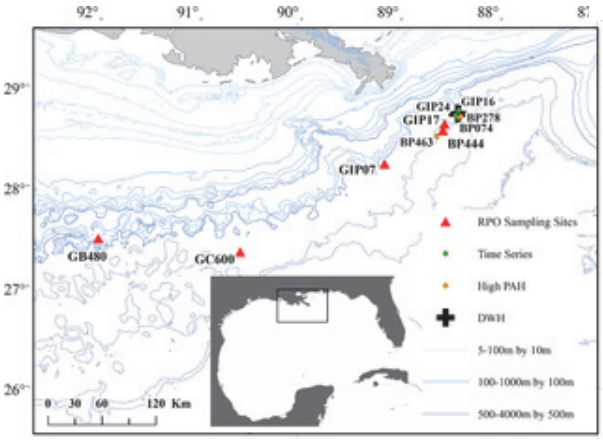

Fig 1.
Sites of sediment collection for time series (green), high PAH (yellow), and RPO analysis (re
https://doi.org/10.1371/journal.pone.0212433.g001

		Latitude	Longitude	RPO and Bulk	Bulk only
GIP07	Time Series	28.2397	-89.1207	2010, 2011, 2014	2016, 2017
GIP 16	Time Series	28.7231	-88.4096	--	2010- 2012, 2014
GIP17	Time Series	28.6373	-88.5188	2010, 2011, 2015	2016, 2017
GIP 24	Time Series	28.7706	-88.3812	--	2010, 2011
BP074	High PAH	28.6995	-88.3812	--	2015
BP278	High PAH	28.7150	-88.3590	--	2015
BP444	High PAH	28.575	-88.5377	2015	2017
BP463	High PAH	28.5140	-88.6005	--	2015
GC600	Seep	27.3645	-90.5629	2014	--
GB480	Control	27.4977	-90.9797	2015	--

https://doi.org/10.1371/journal.pone.0212433.t001

Table 1. Sites examined in this study, measurements performed, location and date.
https://doi.org/10.1371/journal.pone.0212433.t001

The Ramped Pyrolysis/Oxidation System (RPO) at the National Ocean Sciences Accelerator M (NOSAMS) was used to serially oxidize sediments in a controlled environment following the inst Rosenheim et al. [13]. All quartz glassware used in this study was pre-combusted at 850°C for sediment, between ~80–110 mg, depending on the C content, was loaded into a pre-combusted combusted quartz wool, and inserted into the combustion oven, sealed away from atmosphere. small quartz cup and loaded into the quartz tube. A total gas flow of 35 mL/min of helium with 8 sample as the temperature was consistently ramped up to 800–1000°C (5°C /min). Prior to beir evolved CO_2 was measured with a Sable Systems CA-10a CO_2 Analyzer, which was then usec was integrated by cryogenically trapping using N_2(l) over selected temperature intervals based evolution profile, by routing the flowing gases to different traps. Ultimately, the samples were ex line, purified using alternating slurries of isopropanol cooled to liquid-solid phase transition with manometrically using a capacitive diaphragm pressure gauge, and then sealed into a borosilica were reduced to graphite using the hydrogen reduction method [24]. Roughly 10% of CO_2 was process to be analyzed for $\delta^{13}C$. The graphite was analyzed for $\Delta^{14}C$ on the USAMS instrumer [25–26]. Hemingway et al. [27] estimated the contamination blank for a typical RPO analysis on with $\delta^{13}C$ = -29.1± 0.1‰ and potentially $\Delta^{14}C$ = -449 ± 41‰. The blank carbon correction for δ +0.15‰ and Fm ranged from -0.002 to +0.002 ($\Delta^{14}C$ ~ 3–4 ‰) [27]. Due to the small size of the differences in endmembers in this experiment, the data herein were not corrected. Bulk $\Delta^{14}C$ a NOSAMS or the University of Georgia Center for Applied Isotope Studies (UGA) using conventi ^{14}C dating and graphitization approaches [24,28].

Results and discussion

Time series of bulk ^{14}C values

As discerned by increasing isotopic enrichment, we observed recovery of bulk radiocarbon and collected in time series from 4 sites (Fig 2A–2D). In general, all the spill affected sites showed r period. $\Delta^{14}C$ signatures were as low as ~-501‰ (representative of a mixture of 38% ^{14}C-free p 2010, and over time returned towards background values which are estimated to be $\Delta^{14}C$ = -20 oil-spill affected sites present in a fundamentally different manner from seep sites (Fig 2A). Oil s fossil carbon overlying more ^{14}C enriched “younger” C; as also noted by Adhikari et al. [10], wh uniform ^{14}C depleted fossil carbon signature through all depths. In addition to the stratified natu evidence of Macondo hydrocarbons in the particulate phase in the deep-water hydrocarbon plu southwest of the Macondo wellhead [29]. In 2015, the surface sediment $\Delta^{14}C$ signatures of the -187.1 to -467.5‰ (Fig 2E) indicating that not all sites in the northern Gulf of Mexico had fully re Interestingly, at two of the sites, the sediment below the surface layer from 1–2 cm was just as surface with $\Delta^{14}C$ signatures ranging from -257.5 to -369.1‰ (Fig 2E). Below that depth, $\Delta^{14}C$ site) was revisited again in 2017 where we observed baseline values. We further explored the is using RPO to analyze the potential evolution of the sedimented petrocarbon from the time serie

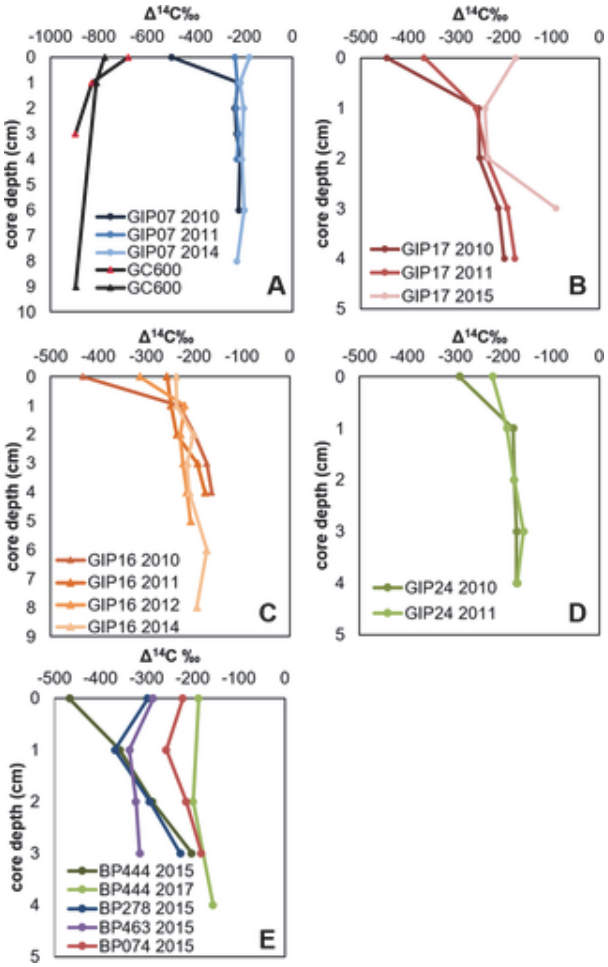

Fig 2. Bulk radiocarbon signatures of time series and high PAH sediment from DWH affected sites and nat
A) GIP07 and replicate cores from mega seep site GC600, B) GIP17, C) GIP16, D) GIP24, E Mason et al. [23] sampled in 2015 and Site BP444 revisited in 2017. Bulk $\Delta^{14}C$ values of sed back to baseline values, while the high PAH sites in E indicate that not all sites had returned
https://doi.org/10.1371/journal.pone.0212433.g002

Changes in patterns of thermal stability

Our second hypothesis was that the oil-residue deposited in the sediment following the oil spill v fresh Macondo oil. The contaminated sites that were run for RPO, GIP17, BP444 and GIP07, al peaks at higher temperatures than the fresh oil (Fig 3). The evolved CO_2 thermographs from se non-oiled (control), were different from the crude oil thermograph, which exhibited two large low and tapered off at higher temperatures (Fig 3A). The thermograph for the seep, GC600, had tw building to a peak at ~460°C, before rapidly falling off (Fig 3A). The petrocarbon present in GC6 thermochemically stable relative to the Macondo crude oil based on these thermographs. In cor from GC600, sediment from the control site, GB480, exhibited a single prominent peak at ~370 shoulders at higher temperatures (Fig 3A). CO_2 thermographs from presumably uncontaminate contaminated sites followed this same pattern yielding a prominent peak at ~370°C at site BP4 sediments from GIP07 in 2014 which had returned to background-like values (Fig 2). We assign sedimentary organic carbon.

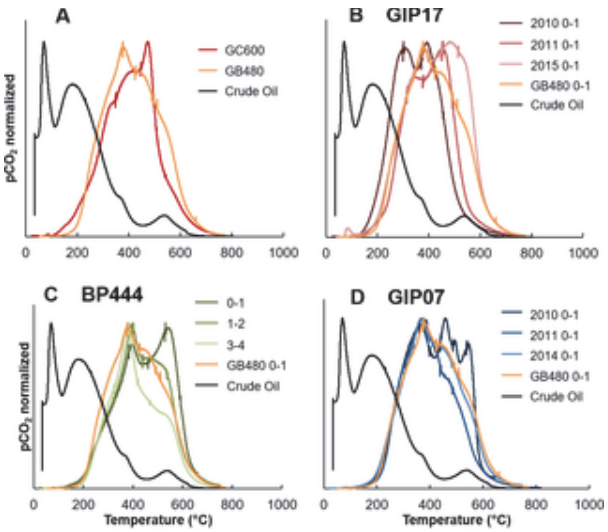

Fig 3. CO_2 evolution thermographs.
A) Crude Oil, Seep site GC600 and Control site GB480, B) GIP17, crude oil and control site, site, D) GIP07, crude oil and control site. Vertical "tic" marks designate temperature boundar
https://doi.org/10.1371/journal.pone.0212433.g003

Our third hypothesis was that there would be a change in CO_2 evolution from lower temperature thermographs as the petrocarbon became increasingly degraded over time. We found evidence the three contaminated sites, GIP17 (Fig 3B) and GIP07 (Fig 3D), and BP444 (Fig 3C). The the contaminated site closest to the well head, had a lower temperature peak straddling 300°C, and similar to the control site. GIP17 profiles from 2011 and 2015 also exhibited the peak at ~370°C higher temperatures over time to 450°C in 2011 and then 480°C in 2015 (Fig 3B). The peaks at the peak evolving at 460°C at the seep site, GC600 (Fig 3A), indicating extremely weathered pe from GIP07 2010, unlike the GIP17 curve, initially exhibited three peaks at higher temperatures >500°C (Fig 3D). CO_2 thermographs from subsequent years at site GIP07 (2011, 2014) are sim prominent peak at 370°C, and the loss of the extra mid-high temperature peaks observed in 20 material evolving at around 500°C would presumably be relatively un-biodegradable, we sugges resuspended.

The depth profile collected in 2015 from site BP444 was similar to GIP07 and GB480, with all d (Fig 3C). BP444 2015 0-1cm had a secondary peak at high temperature ~530°C, which decreas within the core. Considering all the data in Fig 3, we generally observed a peak at 370°C, the co evolved at temperatures below 370°C, or above it, depending upon its "maturity" or evolution to Changes in the magnitude and temperature of evolution of the peaks indicate changes in the th seafloor petrocarbon as it matured from evolving at 300°C, (Fig 3B, GIP17) to over 450–500°C, Pendergraft and Rosenheim [12] observed as we did, that fresh oil evolved CO_2 at temperature that over time, as the oil weathered in the nearshore sediments that they studied, it shifted towa temperatures. Consistent with this interpretation, we observed that at GIP17, over time, and wit CO_2 shifted towards higher temperatures. At GIP07, we believe our sampling effort temporally r temperature evolving petrocarbon, and that our initial sample contained more weathered petroc in 2015. Note the similarity of the samples GIP07, 0–1 in 2010, and GIP17, 0–1 in 2015 (Table 2 are consistent with this interpretation.

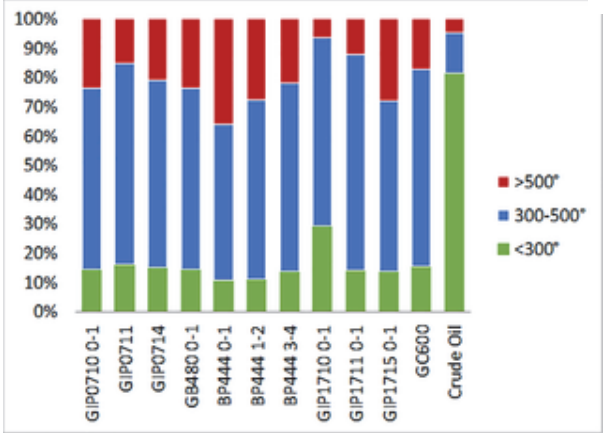

Fig 4. Percent CO_2 evolved from low (300°C), medium (300–500°C) and high (>500°C) temperature.
https://doi.org/10.1371/journal.pone.0212433.g004

	Bulk Measured		Bulk Averaged		Difference	
	$\delta^{13}C$	$\Delta^{14}C$	$\delta^{13}C$	$\Delta^{14}C$	$\delta^{13}C$	$\Delta^{14}C$
GIP07 2010 0–1	-22.8	-501.5	-24.5	-447.5	1.7	-54.0
GIP07 2011 0–1	-21.7	-237.3	-23.4	-247.5	1.7	10.2
GIP07 2014 0–1	-22.2	-177.4	-23.4	-242.2	1.2	64.8
GB480 2015 0–1	-22.2	-132.4	-22.9	-189.4	0.7	57.0
BP444 2013 0–1	-22.1	-467.5	-22.8	-422.4	0.7	-45.1
BP444 2013 1–2	-21.8	-358.1	-22.4	-361.4	0.6	3.3
BP444 2013 3–4	-21.1	-202.1	-21.9	-207.0	0.9	4.9
GIP17 2010 0–1	-23.1	-445.2	-25.2	-491.6	2.1	46.4
GIP17 2011 0–1	-23.8	-368.5	-23.7	-396.1	-0.1	27.6
GIP17 2015 0–1	-23.2	-237.3	-23.2	-264.3	0.0	27.0
GC600 2014 0–1	-29.0	-915.7	-29.4	-912.6	0.4	-3.1

https://doi.org/10.1371/journal.pone.0212433.t002

Table 2. Comparison of bulk measured isotopic values vs RPO weighted average bulk values.
A paired t-test indicated no difference for $\Delta^{14}C$ values, p = 0.259, t = 1.103, while bulk meas significantly enriched relative to the RPO weighted average (p = 0.002, t = 4.158).
https://doi.org/10.1371/journal.pone.0212433.t002

The percent oxidized by the temperature intervals low: <300°C, medium: 300–500°C and high: shifts in the thermochemical stability of the carbon in the sediments through time [12]. These ca CO_2 data continuously collected during RPO prior to purification on the vacuum line. The major oxidized below 300°C, whereas all of the sediment, both oil-contaminated and unaffected, was above 300°C, with only 10–16% oxidized at lower temperatures (Fig 4). Sediment from GIP17 v hypothesis, with 2010 having the most C oxidized <300°C, 29%, decreasing over time to 14% i oxidized at >500°C increased over time from 6% in 2010 to 28% in 2015. The down core profile percentages for C oxidized <300°C, ranging from 11–14%, while at high temperatures (>500°C) oxidized down core from 36% at 0-1cm to 28% at 1-2cm and 22% from 3-4cm. The majority of t of temperatures (300–500°C) throughout all sampling years at all sites, summarized in Table 3.

	<300°C	300–500°C	>500°C
Crude oil	82%	14%	5%
GC600 2014 0–1	16%	67%	17%
GB480 2015 0–1	15%	62%	23%
GIP17 2010 0–1	29%	64%	6%
GIP17 2011 0–1	14%	74%	12%
GIP17 2015 0–1	14%	58%	28%
GIP07 2010 0–1	14%	62%	24%
GIP07 2011 0–1	16%	69%	15%
GIP07 2014 0–1	15%	64%	21%
BP444 2015 0–1	11%	53%	36%
BP444 2015 1–2	11%	61%	28%
BP444 2015 3–4	14%	65%	22%

https://doi.org/10.1371/journal.pone.0212433.t003

Table 3. Percent of CO_2 evolved at low, medium, and high temperatures.
https://doi.org/10.1371/journal.pone.0212433.t003

Relative to Pendergraft et al. [11] and Pendergraft and Rosenheim [12], our thermographs were temperatures, even in 2010, compared to their initial oiled marsh samples, which exhibited CO_2 similar to crude oil. We suggest that degradation of the hydrocarbons en route prior to depositio these differences. Almost half of the hydrocarbons released from the broken well head rose to t before sinking, potentially during a Marine Oil Snow Sedimentation and Flocculent Accumulatio hydrocarbon droplets (<100 μm) suspended in the water, formed a deep-sea plume that travelle Both pools of hydrocarbons were exposed to extensive and rapid degradation while in the oxic dissolution, temperature, and pressure changes [36]. Through microbial processes, hydrocarbo water plume formed aggregates or flocculants, which caused them to sink to the seafloor [1,9,3 the water column than it was following deposition on the seafloor [5,9]. Bagby et al. [9] modeled and found that the size of the oil compound and aggregated particle affected the speed of degra sediment; the larger the particle and compound, the slower the degradation rate. This longer de the seafloor for the deep-water samples accounts for the differences we observe between the c sites and the marsh sediment from Pendergraft and Rosenheim [12].

The difference in the degradation period could account for the differences in the thermographs deposited at GIP07 (~90km from the wellhead), travelled further and therefore degraded more b deposited at GIP17 (~17km from the wellhead). This extended degradation period was reflected temperature differences between the initial sampling years. The thermographs from GIP17 in 2(1–2) from 2015 had more CO_2 evolved at higher temperatures, suggesting they had similar deg

Trends in the $\Delta^{14}C$ composition of evolved CO_2

We observed marked differences between the control (GB480) and seep site (GC600) due to th (GB480) of petrocarbon (Fig 5). Relative to the seep site, the control site had higher $\Delta^{14}C$ value CO_2 from lower temperatures. Evolved CO_2 fractions had decreasing $\Delta^{14}C$ values as temperat fraction was $\Delta^{14}C$ = -316.1‰ (Fig 5A, Tables 2 and 4). The seep site had consistently low value $\Delta^{14}C$ ranging between -881.1 to -950.5‰ over all temperature fractions (Fig 5C). The $\delta^{13}C$ valu first fraction, $\delta^{13}C$ = -25.1‰, then increased at the ~370°C peak, $\delta^{13}C$ = -21.7‰, before decrea 5B). The seep sediments followed a similar pattern, with the lowest being the first fraction, incre decreasing again for the final fraction, however, the $\delta^{13}C$ values of the CO_2 evolved from the se across all fractions, < -28‰ over all temperatures (Fig 5D).

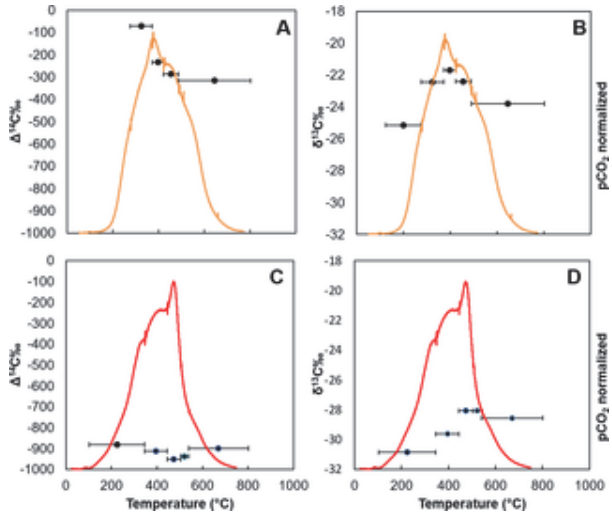

Fig 5. CO_2 thermograph and isotopic composition of evolved CO_2.
Temperature interval of CO_2 fractions indicated by horizontal bars. A) Control site GB480: Δ^{1} C) Seep site GC600 $\Delta^{14}C$, D) Seep site GC600 $\delta^{13}C$.
https://doi.org/10.1371/journal.pone.0212433.g005

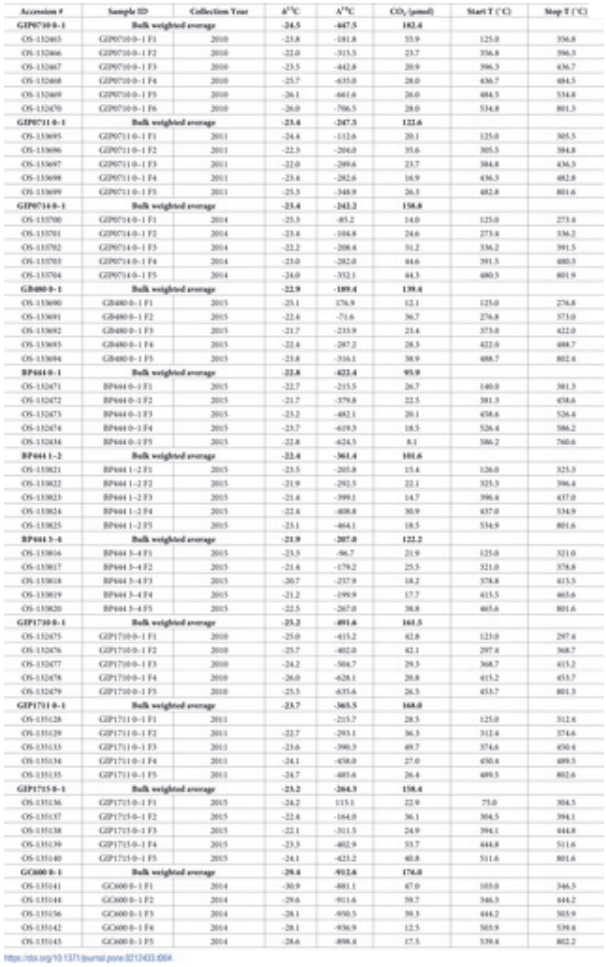

Accession #	Sample ID	Collection Year	$\delta^{13}C$	$\Delta^{14}C$	CO_2 (µmol)	Start T (°C)	Stop T (°C)
GIP0710 0–1	**Bulk weighted average**		**-24.5**	**-447.5**	**182.4**		
OS-132465	GIP0710 0–1 F1	2010	-23.8	-181.8	55.9	125.0	356.8
OS-132466	GIP0710 0–1 F2	2010	-22.0	-313.5	23.7	356.8	396.3
OS-132467	GIP0710 0–1 F3	2010	-23.5	-442.8	20.9	396.3	436.7
OS-132468	GIP0710 0–1 F4	2010	-25.7	-635.0	28.0	436.7	484.5
OS-132469	GIP0710 0–1 F5	2010	-26.1	-661.6	26.0	484.5	534.8
OS-132470	GIP0710 0–1 F6	2010	-26.0	-706.5	28.0	534.8	801.3
GIP0711 0–1	**Bulk weighted average**		**-23.4**	**-247.5**	**122.6**		
OS-133695	GIP0711 0–1 F1	2011	-24.4	-112.6	20.1	125.0	305.5
OS-133696	GIP0711 0–1 F2	2011	-22.3	-204.0	35.6	305.5	384.8
OS-133697	GIP0711 0–1 F3	2011	-21.0	-289.6	23.7	384.8	436.3
OS-133698	GIP0711 0–1 F4	2011	-23.4	-282.6	16.9	436.3	482.8
OS-133699	GIP0711 0–1 F5	2011	-25.3	-348.9	26.3	482.8	801.6
GIP0714 0–1	**Bulk weighted average**		**-23.4**	**-242.2**	**150.8**		
OS-135700	GIP0714 0–1 F1	2014	-25.3	-85.2	14.0	125.0	273.4
OS-135701	GIP0714 0–1 F2	2014	-23.4	-104.8	24.6	273.4	336.2
OS-135702	GIP0714 0–1 F3	2014	-22.2	-208.4	31.2	336.2	391.5
OS-135703	GIP0714 0–1 F4	2014	-23.0	-282.0	44.6	391.5	480.3
OS-135704	GIP0714 0–1 F5	2014	-24.0	-352.1	44.3	480.3	801.9
GB480 0–1	**Bulk weighted average**		**-22.9**	**-189.4**	**139.4**		
OS-133690	GB480 0–1 F1	2015	-25.1	176.9	12.1	125.0	276.8
OS-133691	GB480 0–1 F2	2015	-22.6	-71.6	36.7	276.8	373.0
OS-133692	GB480 0–1 F3	2015	-21.7	-233.9	23.4	373.0	422.0
OS-133693	GB480 0–1 F4	2015	-22.4	-287.2	28.3	422.0	688.7
OS-133694	GB480 0–1 F5	2015	-23.8	-316.1	38.9	688.7	802.6
BP644 0–1	**Bulk weighted average**		**-21.8**	**-622.4**	**93.9**		
OS-132471	BP644 0–1 F1	2015	-22.7	-215.5	26.7	140.0	381.3
OS-132472	BP644 0–1 F2	2015	-21.7	-379.8	22.5	381.3	458.6
OS-132473	BP644 0–1 F3	2015	-23.2	-482.1	20.1	458.6	526.4
OS-132474	BP644 0–1 F4	2015	-23.7	-619.3	18.5	526.4	586.2
OS-132434	BP644 0–1 F5	2015	-22.8	-624.5	8.1	586.2	760.6
BP644 1–2	**Bulk weighted average**		**-22.4**	**-561.4**	**101.6**		
OS-133821	BP644 1–2 F1	2015	-23.5	-205.8	15.4	126.0	325.3
OS-133822	BP644 1–2 F2	2015	-21.9	-292.5	22.1	325.3	396.4
OS-133823	BP644 1–2 F3	2015	-21.4	-399.1	14.7	396.4	437.0
OS-133824	BP644 1–2 F4	2015	-22.4	-408.8	30.9	437.0	534.9
OS-133825	BP644 1–2 F5	2015	-23.1	-464.1	18.5	534.9	801.6
BP644 3–4	**Bulk weighted average**		**-21.9**	**-207.0**	**122.2**		
OS-133816	BP644 3–4 F1	2015	-23.3	-96.7	21.9	125.0	321.0
OS-133817	BP644 3–4 F2	2015	-21.4	-179.2	25.5	321.0	378.8
OS-133818	BP644 3–4 F3	2015	-20.7	-237.9	18.2	378.8	415.5
OS-133819	BP644 3–4 F4	2015	-21.2	-199.9	17.7	415.5	465.6
OS-133820	BP644 3–4 F5	2015	-22.5	-267.0	38.8	465.6	801.6
GIP1710 0–1	**Bulk weighted average**		**-23.2**	**-491.6**	**161.5**		
OS-132475	GIP1710 0–1 F1	2010	-25.0	-415.2	42.8	125.0	297.4
OS-132476	GIP1710 0–1 F2	2010	-25.7	-402.0	42.1	297.4	368.7
OS-132477	GIP1710 0–1 F3	2010	-24.2	-504.7	29.3	368.7	413.2
OS-132478	GIP1710 0–1 F4	2010	-26.0	-628.1	20.8	415.2	453.7
OS-132479	GIP1710 0–1 F5	2010	-25.5	-631.6	26.5	453.7	801.3
GIP1711 0–1	**Bulk weighted average**		**-23.7**	**-365.5**	**168.0**		
OS-135128	GIP1711 0–1 F1	2011		-215.7	28.5	125.0	312.4
OS-135129	GIP1711 0–1 F2	2011	-22.7	-293.1	36.3	312.4	374.6
OS-135133	GIP1711 0–1 F3	2011	-23.6	-390.3	49.7	374.6	450.4
OS-135134	GIP1711 0–1 F4	2011	-24.1	-458.0	27.0	450.4	489.5
OS-135135	GIP1711 0–1 F5	2011	-24.7	-485.6	26.4	489.5	802.6
GIP1713 0–1	**Bulk weighted average**		**-23.2**	**-264.3**	**158.4**		
OS-135136	GIP1713 0–1 F1	2013	-24.2	115.1	22.9	75.0	304.5
OS-135137	GIP1713 0–1 F2	2013	-22.6	-164.0	36.1	304.5	394.1
OS-135138	GIP1713 0–1 F3	2013	-22.1	-311.5	24.9	394.1	444.8
OS-135139	GIP1713 0–1 F4	2013	-23.3	-402.9	33.7	444.8	511.6
OS-135140	GIP1713 0–1 F5	2013	-24.1	-423.2	40.8	511.6	801.6
GC600 0–1	**Bulk weighted average**		**-29.4**	**-913.6**	**176.0**		
OS-135141	GC600 0–1 F1	2014	-30.9	-881.1	47.0	103.0	346.3
OS-135144	GC600 0–1 F2	2014	-29.6	-911.6	59.7	346.3	444.2
OS-135136	GC600 0–1 F3	2014	-28.1	-930.5	39.3	444.2	503.9
OS-135142	GC600 0–1 F4	2014	-28.1	-936.9	12.5	503.9	539.4
OS-135143	GC600 0–1 F5	2014	-28.6	-898.4	17.3	539.4	802.2

https://doi.org/10.1371/journal.pone.0212433.t004

Table 4. Summary of ramped pyrolysis/oxidation (RPO) results.
https://doi.org/10.1371/journal.pone.0212433.t004

We expected the $\Delta^{14}C$ value of the evolved CO_2 at the time series sites (Fig 6) to initially exhib petrocarbon contamination and to increase as petrocarbon degraded or was mobilized from the However, at these sites, typically the first fraction that evolved at the lowest temperatures was t fraction was the most depleted, similar to the control, in terms of $\Delta^{14}C$ (Fig 6 and Table 4). Only trends: GIP17 2010, and GC600, where all temperature fractions were highly depleted in radioc evolved CO_2 fractions of sediment from GIP17 became increasingly enriched over time from 20 6A, 6C and 6E; Tables 2 and 4).

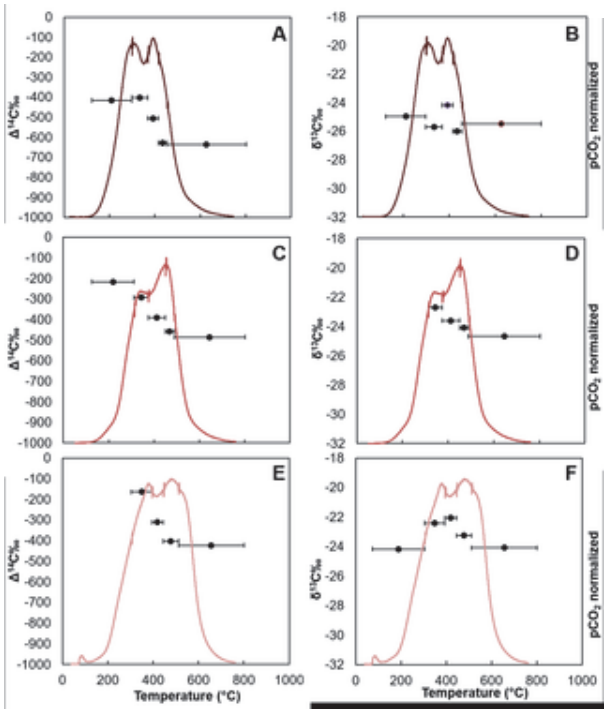

Fig 6. CO_2 thermograph and isotopic composition of evolved CO_2 for site GIP 17.
Temperature interval of CO_2 fractions indicated by horizontal bars. A) GIP17 2010 $\Delta^{14}C$, B) $\delta^{13}C$, C) GIP17 2011 $\Delta^{14}C$, D) GIP17 2011 $\delta^{13}C$, E) GIP17 2015 $\Delta^{14}C$, F) GIP17 2015 $\delta^{13}C$.
https://doi.org/10.1371/journal.pone.0212433.g006

The evolved CO_2 from GIP07 also exhibited the trend of decreasing $\Delta^{14}C$ signatures as temper Table 4). At site BP444 (Fig 8), segment 0-1cm and 1-2cm had similar $\Delta^{14}C$ values at lower ten -205.8‰, but at higher temperatures, the 0-1cm segment was lower than at 1-2cm, with $\Delta^{14}C$ = further down core at site BP444, the evolved CO_2 fractions from sediment collected from 3-4cm the first two segments from 0–1 and 1-2cm, with the initial and final fractions $\Delta^{14}C$ = -96.7 and samples, GB480 and GIP17 2015 0–1 cm (Table 4) exhibited initial CO_2 evolution with high Δ^{14} the deposition of bomb radiocarbon that had been sequestered in the terrestrial environment, e sediments.

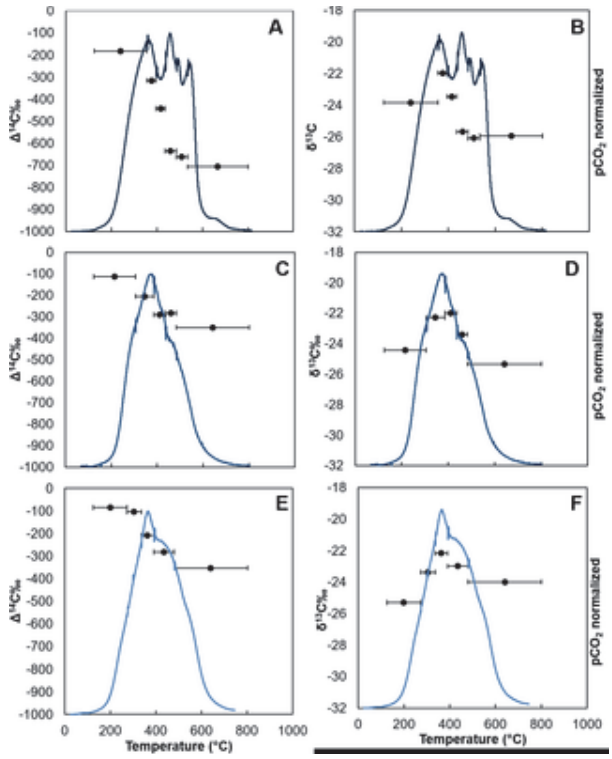

Fig 7. CO_2 thermograph and isotopic composition of evolved CO_2 for site GIP07.
Temperature interval of CO_2 fractions indicated by horizontal bars. A) GIP07 2010 $\Delta^{14}C$, B) ($\Delta^{14}C$, D) GIP07 2011 $\delta^{13}C$, E) GIP07 2014 $\Delta^{14}C$, F) GIP07 2014 $\delta^{13}C$.
https://doi.org/10.1371/journal.pone.0212433.g007

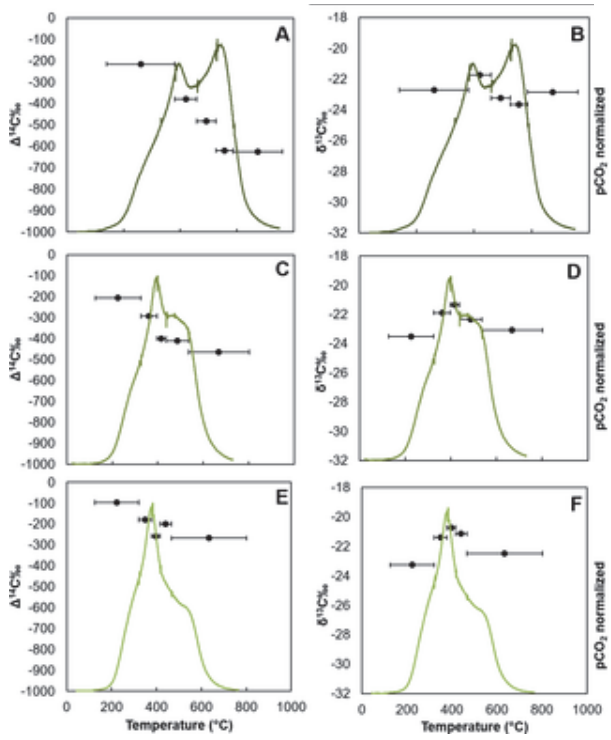

Fig 8. CO_2 thermograph and isotopic composition of evolved CO_2 for high PAH site BP444.
Temperature interval of CO_2 fractions indicated by horizontal bars. A) 0-1cm $\Delta^{14}C$, B) 0-1cm $\delta^{13}C$, E) 3-4cm $\Delta^{14}C$, and F) 3-4cm $\delta^{13}C$.
https://doi.org/10.1371/journal.pone.0212433.g008

Both the level of contamination and the distance from the source played a role in the recovery r
As mentioned previously, higher contamination may slow overall degradation rates, potentially c
sink faster from the water column [9]. Valentine et al. [1] found consistently high levels of hopan
wellhead. Similarly, Adhikari et al. [10] found elevated levels of PAHs < 35km from the well head
sediment beyond this distance returned to background levels. Because the bulk of the oil degra
prior to sedimentation, the further the oil travelled, the more it degraded [4]. This supports our ir
between the thermographs of GIP07 and GIP17. GIP07, ~90km from the well head, has three n
temperatures in 2010 than GIP17, which is closer to the well head, ~16.9km away. This is also
of the first fractions of evolved CO_2 from GIP07 and GIP17.

Trends in the $\delta^{13}C$ composition of evolved CO_2

The trends in the $\delta^{13}C$ values were more variable than the trends seen in the $\Delta^{14}C$ signatures.
sediments followed the general trend of increasing from the lower $\delta^{13}C$ value of the first fractior
higher temperatures. The peak seen at ~370°C in the control and several other samples was of
fractions (e.g., -21.7 to -22.5; Figs 5B, 6B, 6D, 6F, 7D, 7F, 8B, 8D and 8F), suggesting its origin
dominant input term for sedimenting particles [38]. Overall, the bulk mean calculated from all th
from GIP17 and GIP07 were the most depleted in $\delta^{13}C$, becoming more enriched in the followir
Sediments from BP444 had the highest $\delta^{13}C$ values, varying by ~1.1‰ throughout the core, wh
lower than all the other sediment. The stable carbon and radiocarbon isotope signatures for all
summarized in Table 4.

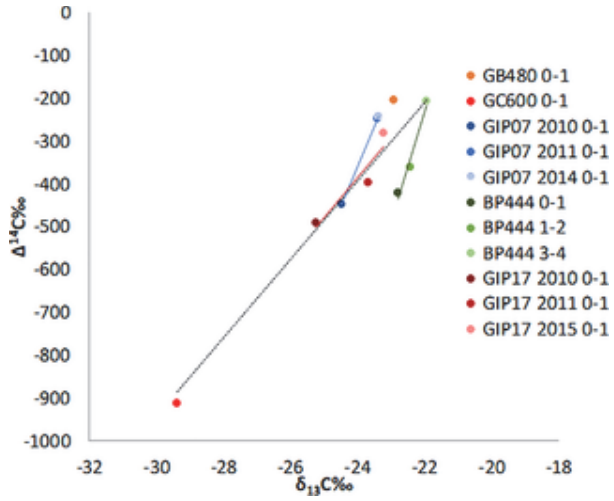

Fig 9. Plot of RPO averaged $\Delta^{14}C$ and $\delta^{13}C$ from each site.
Darker shades are more contaminated, shifting towards lighter shades of the recovered time
(y = 92.295x + 1824.9, r = 0.9187, n = 11, p < 0.0001), time series sediments: Red) GIP17 (y
n = 3, p = 0.0783), Blue) GIP07 (y = 184.68x + 4072.6, r = .9999, n = 3, p < 0.001), Aqua) de
257.42x + 5431.4, r = 0.9843, n = 3, p = 0.0157).
https://doi.org/10.1371/journal.pone.0212433.g009

Several studies have explored the potential of anoxic biodegradation of oil causing enrichment i
Wilkes et al. [39] incubated alkylbenzene utilizing sulfate-reducing bacteria in oil amendments a
compounds at the beginning and ending of the experiment. Wilkes et al. [39] found that as more
heavier the remaining compound reservoir became. Griebler et al. [40] found similar results to W
contaminated site, with specific compounds showing carbon isotope enrichment of the remainin
compounds. Sun et al. [41] found similar increases of the $\delta^{13}C$ of low molecular weight n-alkan
biodegradation, but found no fractionation in high molecular weight compounds even during hea
no change to the bulk $\delta^{13}C$ signatures of the oil, no matter the level of degradation. Whereas th
closed systems, the fractionation of $\delta^{13}C$ during biodegradation of oil, in combination with the m
carbon, could account for the increase we observe in the $\delta^{13}C$ of the evolved CO_2 of sedimente
oil released from the oil spill. The petrocarbon deposited in the GOM was further degraded than
studied. Degradation of organic matter also causes increases in $\delta^{13}C$ values in terrestrial soil sy
results from several studies of well-drained tropical soils where primarily C-3 vegetation derived
degraded down core. The degradation down core caused $\delta^{13}C$ signatures of the remaining orga
[43–45].

Sediment source composition and variation

We calculated the weighted average for $\delta^{13}C$ and $\Delta^{14}C$ per sample, combining the mass-weigh CO_2 fractions; which were not significantly different from the measured bulk signatures for **Δ** ^{14}C we employed a two-endmember mixing model using the **Δ** ^{14}C results to calculate the percent c sources (Table 5). For modern surface sediments we used a value of $\Delta^{14}C$ = ~-200±29‰ [3], a of -1000‰

$$\%_{\text{Modern}} = (|\Delta^{14}C_{\text{petrocarbon}}| + \Delta^{14}C_{\text{Bulk RPO}})/(|\Delta^{14}C_{\text{petrocarbon}}| - \Delta^{14}C_{\text{backgrou}}$$

The results of a two-endmember mixing model followed the trends of the isotopes, with the prop petrocarbon decreasing over time as the isotope signatures increased. Our seep and control sit spectrum with the percent C from modern sources ranging from 11%, at GC600, to 101% at GB -1%, from GB480, to 89% at GC600. GB480 is slightly more enriched than our estimated backg caused it to have over 100% modern sources and below 0% petrocarbon (e.g. 101% and -1%). GIP07 contain 36 and 31%, petrocarbon in 2010 and decreased to 8% and 5% by 2015 and 20 model data are summarized in Table 5. To test for sensitivity, we varied the radiocarbon backgr three sediments from a range of signatures including: background (BP444 2015 3-4cm), mid-ra radiocarbon depleted (GC600). The sediment closest to background had the most potential vari range varied 2–3%, and finally there was no difference in the highly depleted sediment (Table 6

	$\delta^{13}C$	$\Delta^{14}C$	Percent Modern	Percent Petrocarbon
GB480 2015 0–1	-22.9	-189.4	101	-1
GIP17 2010 0–1	-25.2	-491.6	64	36
GIP17 2011 0–1	-23.7	-365.5	79	21
GIP17 2015 0–1	-23.2	-264.3	92	8
GIP07 2010 0–1	-24.5	-447.5	69	31
GIP07 2011 0–1	-23.4	-247.5	94	6
GIP07 2014 0–1	-23.4	-242.2	95	5
BP444 2015 0–1	-22.8	-422.4	72	28
BP444 2015 1–2	-22.4	-361.4	80	20
BP444 2015 3–4	-21.9	-207.0	99	1
GC600 2014 0–1	-29.4	-912.6	11	89

https://doi.org/10.1371/journal.pone.0212433.t005

Table 5. Estimated percent petrocarbon from RPO analyzed sediments using a ^{14}C mass balance with 2 er and background at -200‰.

https://doi.org/10.1371/journal.pone.0212433.t005

		Estimated		Adjusted Background					
				-229‰		-200‰		-171‰	
	$\Delta^{14}C$ ‰	Modern	Petro-carbon	Modern	Petro-carbon	Modern	Petro-carbon	Modern	Petro-carbon
BP444 3–4	-207.0	99%	1%	103%	-3%	99%	1%	96%	4%
GIP17 2010	-491.6	64%	36%	66%	34%	64%	36%	61%	39%
GC600 2014	-912.6	11%	89%	11%	89%	11%	89%	11%	89%

https://doi.org/10.1371/journal.pone.0212433.t006

Table 6. Sensitivity test for 2 end member model estimating percent carbon sources.

https://doi.org/10.1371/journal.pone.0212433.t006

The co-variation of the RPO averaged $\delta^{13}C$ and $\Delta^{14}C$ was consistent with the C isotope deplet of petrocarbon (Fig 9 and Table 2). This co-variation has also been seen for particulate organic estimated recovery rates as defined as increasing isotopic enrichment over time from the linear variation of the averaged RPO values of $\delta^{13}C$ and $\Delta^{14}C$ for the 0–1 cm interval at the GIP17 ar sample number at each site, there was no statistical significance for one of the regressions (GI

used it to estimate what the recovery rates might be. Of the two time series sites, GIP07, ~90km recovery rate at $\Delta^{14}C$ = 46‰ per year (184.68 in 4 years) than GIP17, ~23km away, with $\Delta^{14}C$ (Fig 9). BP444 exhibited increasing $\Delta^{14}C$ values with depth, becoming $\Delta^{14}C$ = 257‰ less deple analyzed. The radiocarbon profile from BP444 showed a distinct depleted layer from 0-2cm ove from 2-4cm. These noticeable layers indicated that there was little to no mixing or bioturbation f to sample collection in 2015.

Adhikari et al. [10] also analyzed DWH affected sediments using RPO and found depleted radic temperature CO_2 fractions. Additionally, they found elevated levels of PAHs near the Macondo Adhikari et al. [10] and Bagby et al. [9] found that in highly contaminated areas, their respective persisted for 3–4 years following the blowout. These estimates are similar to our recovery estim wellhead, which was ~4 years. We found that sites closer to the wellhead, with potentially highe 5–6 years to reach background $\Delta^{14}C$ signatures.

The slower recovery rates at BP444 could be caused by the highly variable sedimentation rates shortly after the blowout. There was increased sedimentation in the Fall of 2010 through early 2 event following the blowout [2], with sedimentation rates ranging between 0.48 to 2.40 g/cm^2/ye returning to pre-spill fluxes of 0.05 to 0.16 g/cm^2/year later in 2011 [48]. The large spatial heterc could have created areas of higher contamination, which would be indicated by lower radiocarb is closer to the wellhead by ~6km, surface sediment from GIP17 in 2015 was more enriched wit sediment from BP444 in 2015, which had $\Delta^{14}C$ = -422‰. Higher contamination levels would ha explaining the lower $\Delta^{14}C$ signatures and slower recovery at BP444 in 2015 [1,9,49]. The mass contaminated material to the seafloor also reduced the size of the benthic community as well as decline in these communities, there was a reduction in the amount of bioturbation in the surface ^{234}Th results [2]. The reduced mixing would also lead to slower $\Delta^{14}C$ recovery times at site BP

An additional consequence of our study is to shed light on the origin of the sedimentary organic Gordon and Goñi [51–53] hypothesized that organic matter characterized as low-lignin, with hig contributed to organic matter deposited in deep water of the northern GOM. They suggested old matter from historic C-4 prairie grasses along the Mississippi River as a potential source of this evidence to support this hypothesis. The $\delta^{13}C$ and $\Delta^{14}C$ values from the CO_2 thermograph of t closely resembles the samples from the deeper sediment at BP444, 3–4 cm, and the GIP07 20 samples are representative of typical Gulf sediments. They all exhibited decreasing $\delta^{13}C$ and **Δ** temperature, contrary to what would have been observed if recalcitrant C-4 organic matter was matter would evolve CO_2 with low $\Delta^{14}C$ and high $\delta^{13}C$ values at higher temperatures. The final from these samples were similar to or more depleted than marine organic matter $\delta^{13}C$ ~ -20‰ a C-4 source with a $\delta^{13}C$ ~ -14‰. The primary source of organic matter to deep water Gulf sedim

Conclusions

Ramped Pyrolysis/Oxidation combined with isotopic analysis of the evolved CO_2 fractions provi degradation over time. Hydrocarbons deposited on the seafloor of the deep-water Gulf of Mexic Compounds of low thermochemical stability were transformed to compounds of higher thermal from hydrocarbon to petrocarbon. The time frame of this evolution appears to depend upon dist distance the oil traveled prior to deposition.

Acknowledgments

AMS samples were run at the University of Georgia Center for Applied Isotopic Studies, and the Accelerator Mass Spectrometry facility (NOSAMS) at Woods Hole Oceanographic. We thank Al

and Mark Roberts. Samples were collected from the RV *Endeavor*, RV *Pelican* and the RV *Wea* and Ryan Sibert and Andy Montgomery for facilitating sample collection. We also thank the Nat Mass Spectrometry Graduate Student Internship Program. We also thank an anonymous reviev comments and suggestions.

References

1. Valentine DL, Fisher GB, Bagby SC, Nelson RK, Reddy CM, Sylva SP, et al. Fallout plume of submerged oil fi 2014; 111(45), 15906–15911. pmid:25349409
View Article • PubMed/NCBI • Google Scholar

2. Brooks GR, Larson R a., Schwing PT, Romero I, Moore C, Reichart GJ, et al. Sedimentation pulse in the NE (blowout. PLoS One. 2015;10(7):1–24. pmid:26172639
View Article • PubMed/NCBI • Google Scholar

3. Chanton J, Zhao T, Rosenheim BE, Joye S, Bosman S, Brunner C, et al. Using natural abundance radiocarbo seafloor following the Deepwater Horizon oil spill. Environ Sci Technol, 2015; 49(2), 847–854. pmid:25494527
View Article • PubMed/NCBI • Google Scholar

4. Stout SA, Rouhani S, Liu B, Oehrig J, Ricker RW, Baker G, et al. Assessing the footprint and volume of oil de Deepwater Horizon oil spill. Mar Pollut Bull 2016; pmid:27677393
View Article • PubMed/NCBI • Google Scholar

5. Stout SA, Payne JR. Macondo oil in deep-sea sediments: Part 1: sub-sea weathering of oil deposited on the s 2016;111(1–2):365–80. pmid:27488960
View Article • PubMed/NCBI • Google Scholar

6. Romero IC, Toro-Farmer G, Diercks AR, Schwing P, Muller-Karger F, Murawski S, et al. Large-scale depositio following a deep-water oil spill. Environ Pollut. 2017; 228:179–89. pmid:28535489
View Article • PubMed/NCBI • Google Scholar

7. Brakstad OG, Lewis A, Beegle-Krause CJ. A critical review of marine snow in the context of oil spills and oil s Deepwater Horizon oil spill. Mar Pollut Bull, 2018; 135, 346–356. pmid:30301046
View Article • PubMed/NCBI • Google Scholar

8. Passow U, Ziervogel K. Marine Snow Sedimented Oil Released During the Deepwater Horizon Spill. Oceano
View Article • Google Scholar

9. Bagby SC, Reddy CM, Aeppli C, Fisher GB, Valentine DL. Persistence and biodegradation of oil at the ocean Acad Sci. 2016; 201610110. pmid:27994146
View Article • PubMed/NCBI • Google Scholar

10. Adhikari PL, Maiti K, Overton EB, Rosenheim BE, Marx BD. Distributions and accumulation rates of polycyclic of Mexico sediments. Environ Pollut. 2016; 212:413–23. pmid:26895564
View Article • PubMed/NCBI • Google Scholar

11. Pendergraft MA, Dincer Z, Sericano JL, Wade TL, Kolasinski J, Rosenheim BE. Linking ramped pyrolysis isot analysis. Environ Res Lett. 2013; 8(November):44038–10.
View Article • Google Scholar

12. Pendergraft MA, Rosenheim BE. Varying relative degradation rates of oil in different forms and environments Technol. 2014; 48(18):10966–74. pmid:25105342
View Article • PubMed/NCBI • Google Scholar

13. Rosenheim BE, Day MB, Domack E, Schrum H, Benthien A, Hayes JM. Antarctic sediment chronology by prc Methodology and data treatment. Geochemistry, Geophys Geosystems. 2008; 9(4):1–16.
View Article • Google Scholar

14. Plante AF, Fernández JM, Haddix ML, Steinweg JM, Conant RT. Biological, chemical and thermal indices of s soils. Soil Biol Biochem. 2011; 43(5):1051–8.
View Article • Google Scholar

15. Aeppli C, Carmichael C a., Nelson RK, Lemkau KL, Graham WM, Redmond MC, et al. Oil weathering after th formation of oxygenated residues. Environ Sci Technol. 2012; 46(16):8799–807. pmid:22809266
View Article • PubMed/NCBI • Google Scholar

16. Ruddy BM, Huettel M, Kostka JE, Lobodin VV, Bythell BJ, McKenna A, et al. Targeted petroleomics: Analytica products from Pensacola Beach. Energy & Fuels 2014; 28(6): 4043–4050.
View Article • Google Scholar

17. Redmond MC and Valentine DL. Natural gas and temperature structured a microbial community response to t Acad. Sci. 2012, 109, 20292–20297. pmid:21969552
View Article • PubMed/NCBI • Google Scholar

18. Dubinsky EA, Conrad ME, Chakraborty R, Bill M, Borglin SE, Hollibaugh JT, et al. Succession of hydrocarbon Deepwater Horizon oil spill in the gulf of Mexico. Environ. Sci. Technol. 2013; 47, 10860–10867. pmid:239371
View Article • PubMed/NCBI • Google Scholar

19. Mason OU, Hazen TC, Borglin S, Chain PS, Dubinsky EA, Fortney JL, et al. Metagenome, metatranscriptome response to Deepwater Horizon oil spill. ISME J 2012; 6, 1715–1727, pmid:22717885
View Article • PubMed/NCBI • Google Scholar

20. White HK, Reddy CM, Eglinton TI. Isotopic constraints on the fate of petroleum residues sequestered in salt n 2005; 39(15), 2545–2551.
View Article • Google Scholar

21. White HK; Reddy CM; Eglinton TI. Radiocarbon-based assessment of fossil fuel derived contaminant associa 2008, 42(15), 5428–5434. pmid:18754456
View Article • PubMed/NCBI • Google Scholar

22. Reddy CM, Pearson A, Xu L, McNichol A, Benner BA, Wise SA, et al. Radiocarbon as a tool to apportion the and black carbon in environmental samples. Environ. Sci. Technol. 2002; 36, 1774–1782. pmid:11998834
View Article • PubMed/NCBI • Google Scholar

23. Mason OU, Scott NM, Gonzalez A, Robbins-Pianka A, Bælum J, Kimbrel J, et al. Metagenomics reveals sedi Deepwater Horizon oil spill. ISME J, 2014; 8(7), 1464–1475. pmid:24451203
View Article • PubMed/NCBI • Google Scholar

24. Pearson A, McNichol AP, Schneider RJ, von Reden KF, Zheng Y. Microscale AMS ^{14}C measurement at NOS
View Article • Google Scholar

25. von Reden KF, Donoghue JC, Elder KL, Gagnon AR, Gerlach DS, Griffin VS, et al. Plans for expanded ^{14}C a progress report. Nucl Instruments Methods Phys Res, 2004; 223–224, 50–54
View Article • Google Scholar

26. Longworth BE, von Reden KF, Long P, Roberts ML. A high output, large acceptance injector for the NOSAMS Methods Phys Res, 2015; 361, 211–2016
View Article • Google Scholar

27. Hemingway JD, Galy VV, Gagnon AR, Grant KE, Rosengard SZ, Soulet G, et al. Assessing the blank carbon kinetic isotope fractionation of the ramped pyrolysis/oxidation instrument at NOSAMS. Radiocarbon, 2017; 59
View Article • Google Scholar

28. Choi Y, Wang Y, Dynamics of carbon sequestration in a coastal wetland using radiocarbon measurements. *Gl* 1–12.
View Article • Google Scholar

29. Fernández-Carrera A, Rogers KL, Weber SC, Chanton JP, Montoya JP. Deep Water Horizon oil and methane Mexico. Limnol. Oceanogr. 2016, 61, S387–S400.
View Article • Google Scholar

30. Atlas RM, and Hazen TC. Oil biodegradation and bioremediation: a tale of the two worst spills in U.S. history. pmid:21699212
View Article • PubMed/NCBI • Google Scholar

31. Diercks AR, Highsmith RC, Asper VL, Joung DJ, Zhou Z, Gou L, et al. Characterization of subsurface polycyc Horizon site. Geophys Res Lett. 2010; 37(L20602)
View Article • Google Scholar

32. Zhou Z, Guo L, Shiller AM, Lohrenz SE, Asper VL, Osburn CL. Characterization of oil components from the D Mexico using fluorescence EEM and PARAFAC techniques. Mar Chem. 2013; 148(0) 10–21
View Article • Google Scholar

33. Passow U, Ziervogel K, Asper V, Diercks A. Marine snow formation in the aftermath of the Deepwater Horizor

Lett, 2012; 7(3), 1–11.
View Article • Google Scholar

34. Passow U. Formation of rapidly-sinking, oil-associated marine snow. Deep Res Part II Top Stud Oceanogr, 20
View Article • Google Scholar

35. Valentine DL, Kessler JD., d MC, Mendes SD, Heintz MB, Farwell C, et al. Propane respiration jump-starts mi
(New York, N.Y.), 2010; 330(6001), 208–11. pmid:20847236
View Article • PubMed/NCBI • Google Scholar

36. Reddy CM, Arey S, Seewald JS, Sylva SP, Lemkau KL, Nelson RK, et al. Composition and fate of gas and oil
Deepwater Horizon oil spill. Proc Natl Acad Sci, 2012; 109(50): 20229–20234. pmid:21768331
View Article • PubMed/NCBI • Google Scholar

37. Diercks AR, Dike C, Asper VL, DiMarco SF, Chanton JP, Passow U. Resuspension scales in the northern Gul
View Article • Google Scholar

38. Chanton JP, Giering SL Bosman S, Rogers K, Sweet J, Asper V, et al. Isotope Composition of Sinking Particle
the Gulf of Mexico, 2010–2015. Elem Sci Anth. 2018; 6, 43
View Article • Google Scholar

39. Wilkes H, Boreham C, Harms G, Zengler K, Rabus R. Anaerobic degradation and carbon isotopic fractionatio
reducing bacteria. *Org Geochem*, 2000; 31(1), 101–115.
View Article • Google Scholar

40. Griebler C, Safinowski M, Vieth A, Richnow HH, and Meckenstock RU. Combined Application of Stable Carbo
Determination for Assessing In Situ Degradation of Aromatic Hydrocarbons in a Tar Oil-Contaminated Aquifer
pmid:14750740
View Article • PubMed/NCBI • Google Scholar

41. Sun Y, Chen Z, Xu S, Cai P. Stable carbon and hydrogen isotopic fractionation of individual n-alkanes accomp
group of progressively biodegraded oils. Org Geochem, 2005; 36(2), 225–238.
View Article • Google Scholar

42. Wynn JG. Carbon isotope fractionation during decomposition of organic matter in soils and paleosols: Implica
paleosols. Palaeogeogr, Palaeoclimatol, Palaeoecol, 2007; 251(3–4), 437–448.
View Article • Google Scholar

43. Krull ES, Bestland EA, Gates WP, Soil organic matter decomposition and turnover in a tropical Ultisol: Eviden
Radiocarbon. 2002; 44, 93–112
View Article • Google Scholar

44. Krull ES, Skjemstad JO, Burrows WH, Bray SG, Wynn JG, Bol R, et al. Recent vegetation changes in central
and 14C analyses of soil organic matter. Geoderma 2005; 126(3–4), 241–259

View Article • Google Scholar

45. Wynn JD, Harden JW, Fries TL. Stable carbon isotope depth profiles and soil organic carbon dynamics in the 2006;131, 89–109.
View Article • Google Scholar

46. Chanton JP, Cherrier J, Wilson RM, Sarkodee-Adoo J, Bosman S, Mickle A. Radiocarbon evidence that carbc the planktonic food web of the Gulf of Mexico. Environ Res Lett, 2012; 7
View Article • Google Scholar

47. Cherrier J, Sarkodee-Adoo J, Guilderson TP, Chanton JP. Fossil Carbon in Particulate Organic Matter in the C Horizon Event. Environ Sci Technol Lett, 2014; 1(1), 108–112.
View Article • Google Scholar

48. Daly KL, Passow U, Chanton J, Hollander D. Assessing the impacts of oil-associated marine snow formation Deepwater Horizon oil spill. Anthropocene, 2016; 13, 18–33.
View Article • Google Scholar

49. Montagna PA, Baguley JG, Cooksey C, Hartwell I, Hyde LJ, Hyland JL, et al. Deep-Sea Benthic Footprint of tl 2013; 8(8).
View Article • Google Scholar

50. Baguley JG, Montagna PA, Cooksey C, Hyland JL, Bang HW, Morrison C, et al. Community response of deep the Deepwater Horizon blowout and oil spill. Mar Ecol Prog Ser, 2015; 528, 127–140.
View Article • Google Scholar

51. Goñi MA, Ruttenberg KC, Eglinton TI. Source and contribution of terrigenous organic carbon to surface sedim 389(6648), 275–278.
View Article • Google Scholar

52. Goñi MA, Ruttenberg KC, Eglinton TI. A reassessment of the sources and importance of land-derived organic Mexico. Geochim Cosmochim Acta, 1998; 62(18), 3055–3075.
View Article • Google Scholar

53. Gordon ES, and Goñi MA. Controls on the distribution and accumulation of terrigenous organic matter in sedi river margin. *Mar Chem*, 2004; 92(1–4), 331–352.
View Article • Google Scholar